Optical Imaging of the Small Intestine Immune Compartments Across Scales

Arielle Planchette
École Polytechnique Fédérale de Lausanne https://orcid.org/0000-0001-6274-6586
Cédric Schmidt
HEPIA/HES-SO, University of Applied Sciences of Western Switzerland
Olivier Burri
École Polytechnique Fédérale de Lausanne
Mercedes Gomez de Agüero
Institute for Systems Immunology, Max Planck research group, University of Würzburg, Germany
https://orcid.org/0000-0002-7132-290X
Aleksandra Radenovic (aleksandra.radenovic@epfl.ch)
École Polytechnique Fédérale de Lausanne https://orcid.org/0000-0001-8194-2785
Alessio Mylonas
École Polytechnique Fédérale de Lausanne https://orcid.org/0000-0001-6220-1973
Extermann Extermann
HESSO / HEPIA https://orcid.org/0000-0002-5858-1122

Article

Keywords: small intestine, Isolated Lymphoid Follicles, microscopy

Posted Date: December 1st, 2021

DOI: https://doi.org/10.21203/rs.3.rs-1046138/v1

Version of Record: A version of this preprint was published at Communications Biology on March 31st, 2023. See the published version at https://doi.org/10.1038/s42003-023-04642-3.

Abstract

The limitations of 2D microscopy constrain our ability to observe and understand tissue-wide networks that are, by nature, 3-dimensional. Optical projection tomography enables the acquisition of large volumes (ranging from micrometres to centimetres) in various tissues, with label-free capacities for the observation of auto-fluorescent signals as well fluorescent-labelled targets of interest in multiple channels. We present a multi-modal workflow for the characterization of both structural and quantitative parameters of the mouse small intestine. As proof of principle, we evidence its applicability for imaging the mouse intestinal immune compartment and surrounding mucosal structures. We quantify the volumetric size and spatial distribution of Isolated Lymphoid Follicles (ILFs) and quantify density of villi throughout centimetre long segments of intestine. Furthermore, we exhibit the age- and microbiota-dependence for ILF development, and leverage a technique that we call reverse-OPT for identifying and homing in on regions of interest. Several quantification capabilities are displayed, including villous density in the autofluorescent channel and the size and spatial distribution of the signal of interest at millimetre-scale volumes. The concatenation of 3D image acquisition with the reverse-OPT sample preparation and a 2D high-resolution imaging modality adds value to interpretations made in 3D. This cross-modality referencing technique is found to provide accurate localisation of ROIs and to add value to interpretations made in 3D. Importantly, OPT may be used to identify sparsely-distributed regions of interest in large volumes whilst retaining compatibility with high-resolution microscopy modalities, including confocal microscopy. We believe this pipeline to be approachable for a wide-range of specialties, and to provide a new method for characterisation of the mouse intestinal immune compartment.

Introduction

The intestine forms an interface between the external environment and the rest of the body, fulfilling many essential functions in the process. Among these are immune system education, and the regulation of the microbiome – which are incidentally interdependent[1,2]. Indeed, we now know that the microbiome is necessary for the correct education of the immune system[3,4] and that this has long-term repercussions on immunity in the gut. As such, the gut microbiome has been linked to distinctly immune-related disorders ranging from obesity[5] and diabetes[6] to auto-immune[7] and allergic diseases[8–10]. Importantly, significant advances in the aetiology of such disorders were made through studying gut structure[11–13]. For example, deficits in gut morphology and barrier permeability have been implicated in both obesity[14,15] and diabetes[16], with the latter showing signs of decline prior to type-1-diabetes onset in non-obese diabetic mice (NOD). The relevance of observing cell localization within tissue regions of the gut is further exemplified by microscopic observations of intraepithelial lymphocyte localisation, which highlighted the impact of high-fat-diet-induced obesity on the control of pathogen transepithelial migration and the mediation of intestinal epithelial repair[15].

Secondary and tertiary lymphoid structures (LT) are strategically positioned along the gastrointestinal tract to orchestrate immuno-surveillance against pathogens and invading microorganisms. These are known to develop during early life[17], and to require stimuli from the microbiome[18,19]. Peyer's patches (seconday LT) and isolated lymphoid follicles (ILFs, tertiary LT) form key networks where microbial antigens are presented to T- and B-cells, effectively dictating both regulation and tolerance to commensals. While new methods are continuously being developed for immuno-phenotyping and isolation of immune cells from ILFs[20,21], their function – deriving from their location at the interface with the microbiota – also necessitates further research in their natural context. Concurrently, the awareness that gut spatial structures have a powerful impact on establishing and sustaining the signaling and metabolic exchanges demanded techniques that will deliver in large-area, volumetric mapping. Existing solutions include confocal microscopy in combination with FISH[22] and lattice light-sheet microscopy[23].

Optical projection tomography (OPT) is a 3D imaging modality that is ideal for mesoscale imaging, offering broad applicability while maintaining compatibility with other microscopy techniques. With fields of view spanning from a few millimetres to 60mm in length[24] and full 3D-volume acquisition times ranging from minutes to an hour[25], OPT is a time- and cost-effective technique with which large-scale structural and functional parameters can be imaged. OPT has been leveraged for concatenated, functional multi-channel plant imaging[24], functional cell proliferation imaging in zebrafish[26], multi-orientation digital sectioning of whole mouse embryos[27] and mouse organ imaging of the liver, pancreas[25] and brain[28].

Recently, we developed a multi-spectral OPT modality to image the mouse gut[29], with a 3D resolution of 28µm allowing the distinction of mucosal layers and villi in samples several centimetres in length. To demonstrate the wide range of applications for this method, we present a workflow that enables mesoscale observation of signal distribution throughout millimetre-long gut sections with autofluorescent contextualization, as well as the identification of regions of interest that can be characterized at higher-resolution following reverse OPT (RevOPT) processing. We apply this workflow to visualise the gut immune compartment and present the first observation of isolated lymphoid follicle (ILF) distribution in a single acquisition spanning several millimetres of gut tissue. Furthermore, we confirm the lack of large organised lymphoid structures in young SPF and old germ-free mice, likely reflecting the age- and microbiome-dependence of the gut immune system development. Finally, by implementing RevOPT and subsequent confocal microscopy, we show the feasibility of tracking regions of interest (ROIs) initially selected in 3D for subsequent higher resolution imaging using traditional histology methods. This method is a powerful approach to characterizing tissues at multiple scales while providing high resolution data with ready-to-use processing pipelines optimized for the mouse gut.

Results

3.1 Sample preparation pipeline and the power of tissue autofluorescence

To achieve the multi-scale observation of spatially-distributed biological signals of interest, we developed a sample preparation pipeline that includes two imaging modalities: high-volume optical projection tomography and high-resolution confocal microscopy after reverse OPT (RevOPT, Fig. 1). The pipeline is divided into four phases, sample preparation (**Fig. 1 a-k**), imaging and image processing (**Fig. 1 l-m**), reverse OPT (**Fig. 1 n-r**) and secondary imaging (**Fig. 1 s**), spanning a duration of approximately three weeks. First, tissue preservation, autofluorescence quenching and tissue permeabilisation are performed to prepare the samples for staining. This is followed by fluorescent antibody staining of select markers. A clearing step precedes the acquisition of optical projections over a 360° sample rotation. Next, a filtered back-projection algorithm is used to reconstruct the projections into a 3D image as described previously[29]. Using RevOPT we revert the sample to a state compatible with freezing in Optimal Cutting Temperature (OCT) compound, allowing for cryostat sectioning and counterstaining (**Fig. 1, p-r**). Finally, in amongst several methods requiring thin sectioning including electron microscopy or single-molecule FISH, we selected confocal microscopy to image regions of interest identified by OPT with improved resolution.

Tissue autofluorescence is an inherent signal produced by extracellular matrix components and certain pigmented cell types. In OPT, autofluorescence quenching is required to reduce noise and retain targeted fluorescent signals[29] (**F**ig. 1, steps **a** and **c**). However, low levels of autofluorescence enable the discrimination of the outer and inner layers of the gut when samples are illuminated at 415nm spectrally filtered between 400-440nm, whilst emission is collected within the range of 455-520nm[29]. A longitudinal portrayal of the gut (**Fig. 2a**) provides an overview of the structures present in the tissue. In reconstructions made up of 1200 projections, well-resolved villi can be observed in a 3D visualisation software (**Fig. 2b**). When taking a cross-sectional view, the mucosal layers can be distinguished from the villi in the OPT scan (**Fig. 2c;** mu = muscularis, sm = submucosa, m = mucosa and L = lumen) whilst a greater resolution is achieved by confocal microscopy on the same sample having undergone RevOPT (**Fig. 2d**). During RevOPT, counterstaining is possible and demonstrated here by the staining of DNA with DAPI (**Fig. 2d**). The improved preservation of cross-sectional structure in OPT is evident when comparing the virtual section (**Fig. 2c**) and its histological counterpart (**Fig. 2d**), with loss of tissue and distortion being apparent in the confocal image.

We implemented a virtual unfolding technique[30] (for more detail, see supplementary **SI Fig. 1**) to observe the gut tissue from within the lumen, with sections spanning from this point to the serosa (**Fig. 2e**, section closest to lumen). Villous density could be calculated by segmenting the unfolded image and finding local maxima (**Fig. 2f**). This can be performed for the whole tissue region or applied to smaller regions of interest to probe different areas of the tissue. In this healthy tissue, overall villous density is mostly homogeneous (**Fig. 2f)**. This data can be transformed into a quantitative visualisation of different sectors (**Fig. 2g**). Virtual unfolding also yields a straightened image (**Fig. 2h**) of the tissue cross section seen in **Fig. 2c**.

Virtual unfolding of 3D-reconstructed data can lead to detailed visualizations of structures that are difficult to visualise in a 3D image such as **Fig. 2a** or in a virtual cross-section as in **Fig. 2c**. We found a

suspected lymphoid follicle in the autofluorescence channel of a different sample (top view **Fig. 2i,** side view **Fig. 2j**), whose structural context is made clear by virtual unfolding (**Fig. 2k** and straightened **Fig. 2l**). The follicle is made up of three lobes, with a concentration of fluorescent vessels in the centre. In the areas surrounding the follicle, gaps in the villi suggests the potential presence of lymphatic vasculature. Typically, large vascular networks are difficult to observe by visualization of cross-sections. In **Fig. 2m,** an example of such a network is shown, highlighting the added value that processing the autofluorescence channel can bring to gut structure characterization.

3.2 Cell-type specific signal distribution throughout the gut volume

OPT can also be used for visualisation of cell types according to stainings of selective markers. To demonstrate this, we chose to stain the gut immune compartment, due to its structured organisation under healthy conditions and its common deregulation in intestinal diseases (e.g. IBD[31]) and other systemic disorders (e.g. metabolic diseases[32,33], autoimmunity[34] and neurodegeneration[35,36]). For this we stained CD45-positive cells using fluorescently labelled antibodies. In healthy adult mice, immune cells are found interspersed at regular intervals or compartmentalised in gut-associated lymphoid structures (GALTs) known as isolated lymphoid follicles (ILFs, **Fig. 3a** triangle). Overlaying the autofluorescence channel reveals other adjacent structures such as blood vessels and luminal dietary fibers (**Fig. 3a**, cross and square respectively). In order to view the three-dimensional characteristics of such an OPT image, a movie is provided in the supplementary information (**SI Movie 1**).

It is known that age- and microbiota-dependent education of the immune system is responsible for the formation of lymphoid structures such as Peyer's patches and ILFs[37,38]. We confirm that with OPT, we are able to identify differences in the immune cell compartments in the contexts of young (14 days) SPF mice and old (30+ weeks) germ-free mice (**Fig. 3b** and **3c** respectively), compared to the old SPF sample shown in **Fig. 3a**. At a young age under normal rearing conditions, no dense regions of immune cells are observed (**Fig. 3b**). Intestines of older, germ-free mice also exhibit reduced CD45-positive cell clusters in the mucosal layers. A two-channel cross-sectional view of these samples (**Fig. 3d-f)** frames the immune signal within the structured layers of the gut. An isolated lymphoid follicle is located within the sub-mucosal layers and is surrounded by smaller, less dense CD45-positive clusters in figure **3d**. Conversely, there is no specific fluorescence in both old germ-free and young SPF animals, thus indicating a lack of well-defined GALT structures in these mouse models (**Fig. 3b, 3c, 3e,** and **3f**).

OPT reconstructions can thus be used for broader, organ-scale characterisation of the mouse intestine. Furthermore, current 3D image processing tools allow for accurate quantification of different parameters. We segmented the ILFs in the 625nm channel alone (**Fig. 3g**) and found their size ranges from approximately 1 to 5 million μm^3 (**Fig. 3h**). Their spatial distribution along the small intestine is uniform, averaging at 500µm in between ILFs (**Fig. 3i**).

3.3 gutOPT pipeline for multi-modal imaging and high resolution characterisation of the gut

Because sample preparation for optical projection tomography is compatible with downstream processing for additional imaging modalities, we wondered whether we could incorporate a single pipeline for imaging at different scales. We performed reverse-OPT (**Fig. 1 n** and **o**) on the samples shown in **Fig. 3** and imaged them using confocal microscopy (**Fig. 4**).

We wondered whether we could use OPT to pre-select regions of interest, and retrace them and image them using high-resolution techniques. To do this, we selected isolated lymphoid follicles in the OPT reconstruction and calculated their distance from the edge of the sample (**Fig. 4a i** and **ii**). Once samples had undergone RevOPT and were mounted in optimal cutting temperature (OCT) compound, the depth of each cryosection was used to track the localization of the ROIs. We find that the fluorescence signal was maintained from the OPT staining, and sections do not require further immuno-staining for confocal imaging.

Specifically, we find that preselected ILF regions observed by OPT are high-density cell clusters rich in CD45-positive cells (**Fig. 4b** and **c**). In both ROIs containing ILFs, the calculated distances were accurate, and we find the immune cell-dense region situated within the submucosa as expected from the OPT reconstructions and their known localisation[39,40]. Areas lacking GALTs in 3D (**Fig. 4a iii**) only contain sparse positive cells in the lamina propria at higher resolution (**Fig. 4d**). By measuring the immune cell density in the whole-sectioned GALT regions we find that the signal density threshold for visibility in OPT is approximately 400 fluorescent cells per mm^2 of DAPI signal (**Fig. 4e**). We imaged the adult germ-free mice that display no GALTs by OPT (**Fig. 4f)**. Here, we find no CD45+ cells along the length of the villi nor in the submucosa, confirming that no ILFs are present, and suggesting that the lack of a microbiome indeed alters the immune compartment in the gut (**Fig. 4f**, triangle). The number of immune cells is also significantly reduced compared to that observed in the gut of SPF mice (**Fig. 4g**). Thus, OPT can be used to identify specific structures and markers of interest using tissue-wide staining, and given a sufficiently dense fluorescent signal ROIs can be traced by confocal microscopy using RevOPT and cryosectioning.

Discussion

The choice of microscopy technique for gut characterization relies on certain features of the signal of interest, including the scale, the required resolution, the need for staining, the sample preparation and its application *in-vivo* or *ex-vivo*. In studying the gut, common imaging techniques include confocal microscopy, light sheet fluorescence microscopy and two-photon microscopy whose applications range from studying villous vascularisation[41], structural integrity[30,42], local inflammatory status[43] and microbial community dynamics[23]. The heterogeneity of gut tissue structure and the dynamic recruitment and trafficking of cells involved in gut health makes 3D microscopy particularly adapted for this setting. In addition, volumetric imaging modalities are continually being developed in parallel with advanced image processing techniques[44–46], as the weight of data grows rapidly with 3D imaging.

We describe a multi-scale and multi-modal pipeline for visualising the gut architecture and associated isolated lymphoid follicles (ILFs) at the scale of organs. We provide quantifications of volumetric sizes

and spatial distribution of ILFs in adult mice throughout centimetre lengths of mouse intestine. We leverage the 3-dimensional nature of OPT data to facilitate the observation of vascular networks in the submucosa, as shown by virtual unfolding. As proof-of-concept, we have evidenced the requirement of the microbiome for the maturation of ILFs, and during development. Finally, we have incorporated a technique – which we have called RevOPT – for higher-resolution imaging of selected ROIs. This bridges imaging of tissue at the organ and histology level, and allows quantitation at different scales. While this method requires specialized manipulation lasting up to three weeks, the gain in information and wide field of view is attractive for studying the distribution and localisation of distinct cellular structures.

Tissue autofluorescence serves multiple roles in the interpretation of microscopy images. It can provide crucial contextualization for fluorescent labels within tissues and facilitate the interpretation of functionality based on fluorescent signals. In addition, the intestinal architecture observed by autofluorescence imaging provides a label-free method for the characterization of diverse parameters[47] which may be used as comprehensive measures of gut integrity and leakiness[48]. Such a technique could be applied to histopathologic scoring where structural deformation is symptomatic of disease. For example, coeliac disease (CD) is characterized by a destruction of the intestinal epithelium driven by gluten-activated inflammation, resulting in observable villous atrophy and lymphocytic infiltration of the epithelium, as shown recently in a novel mouse model of CD[49]. Current methods for the diagnosis of coeliac disease rely heavily on histological observations of prepared endoscopic biopsies, with a necessity for multiple collections due to non-homogeneous tissue alterations[50]. With the ability to accurately reconstruct mesoscale volumes, the presented optical projection tomography pipeline offers an alternative approach that maintains structural integrity whilst multiplying the field of view available for diagnostic observation.

The gastrointestinal tract constitutes an essential site for crosstalk between the external environment and the host, and which dictates immune development[51,52]. Gut immunity is implicated in intestinal diseases, such as inflammatory bowel disease (IBD)[53], and to systemic disorders ranging from metabolic diseases such as diabetes[54] to neurodevelopmental, neuroinflammatory, and neurodegenerative diseases[55–58]. Thus, imaging and characterizing gut-associated lymphoid structures (GALT) is important for understanding how immune development impacts health. Yet, the spatial distribution of immune structures in the gut is not well documented at the mesoscale. To our knowledge, our method is the first to image GALTs in 3D at a centimetre scale, with subsequent high-resolution 2D ROI referencing.

In order to show the applicability of OPT to characterize the mesoscale organization of cell-types within tissues, we explored the development of GALTs in models where age and the microbiota are manipulated. We stained the CD45 antigen that is found on hematopoietic cells[59] from which almost all immune cell types are derived[60]. CD45-rich regions identified as isolated lymphoid follicles (ILF) were found in the gut of a 30-week-old SPF C57BL6 mice. ILFs are a sub-category of gut-associated lymphoid tissues[40] whose functions are to limit contact between luminal microbiota and the epithelium via IgA secretion, and to sense epithelial breaching by bacteria and signal the need for phagocytosis to surrounding

macrophages[61]. These are thought to depend on fibroblastic reticular cells (FRCs) and follicular dendritic cell (FDC)-like fibroblasts, to be seeded by Lymphoid Tissue inducer (LTi) cells, and to require microbiota-induced IL-25 and IL-23[62]. Yet the exact mechanism remains to be fully elucidated and their development characterized along long stretches of the intestine in 3D. For the first time, we are able to measure the variation in volume and the spatial distribution of ILFs in 3D throughout an uninterrupted section of tissue at the millimetre scale. This technique may prove useful in the tissue-wide imaging and characterisation LTi cell clusters and their development into mature GALTs. Furthermore, with concatenated overlapping data acquisition, this is easily extended to the centimetre scale.

The age- and microbiome-dependence of the maturation and regulation of gut immune responses has become evident in recent years[63]. Initial exposure to a microbial environment during the neonatal period shapes the immune system throughout development[64]. In accordance with this, we find a sparse immune signal in young SPF mice, with no discernible GALTs. In addition, the study of germ-free and gnotobiotic models has proven that the gut microbiota is necessary for the development of a mature and complete immune system[65], with post-gnotobiotic colonization with commensal bacteria resulting in the acute induction of lymphoid tissue genesis[19]. Thus, the lack of isolated lymphoid follicles in the small intestine of old germ-free mice observed in OPT is indicative of the expected stunted immune germ-free phenotype.

We also demonstrate the traceability of ROIs between imaging modalities by selecting ILFs in OPT reconstructions and performing RevOPT and confocal microscopy. The distances measured by image processing and by tracking the number of sectioning depths leads to an accurate correlation of signal localization. With signal density quantification, we are able to determine a limit of detection for regions of interest in OPT scans that may become a benchmark for the selection of targets of interest for OPT imaging. RevOPT adds value to our pipeline as it addresses the need for microscopic analysis of biological landscapes whilst offering the opportunity to interpret signals at the mesoscale.

Collectively, we provide an imaging pipeline for versatile multi-modal imaging of the mouse intestine and its associated immune compartment. Furthermore, we demonstrate its ability to quantitatively characterise sparsely distributed structures throughout centimetre long segments of the intestine, in volumetric terms. Cut-free sections reduce the presence of common artefacts that distort the sample and impede large-scale histopathological interpretations. The virtual sections also simplify the registration of multiple imaging depths for 3D or concatenated 2D segmentation of regions of interest, as we have demonstrated here. Finally, we demonstrate the advantage of combining of OPT with RevOPT for the empirical selection of regions of interest for high-resolution downstream imaging. We believe the ease of implementation and the resulting possibilities of analysis in large volumes and at high resolution make the gutOPT pipeline an attractive method for preclinical characterization of gut tissues in mice. Its potential for implementation in whole human tissue biopsy imaging raises exciting prospects for clinical diagnostics. Thus, gutOPT addresses the need for a detailed yet holistic approach to understanding the complex physiological interactions involved in gut health and disease.

Methods

5.1 Animal handling

Specific pathogen free C57BL/6J mice were purchased and housed at the École Polytechnique Fédérale de Lausanne (Switzerland) under specific pathogen free conditions with *ad libitum* access to food and water, according to guidelines and regulations of the state of Vaud, Switzerland (authorization VD3448). Germ-free C57BL/6J mice were obtained from the Clean Mouse Facility, University of Bern (Switzerland). Germ-free status was routinely monitored by culture-dependent and -independent methods and confirmed to be microbial-free. Experiments were performed in accordance with regulations approved by the ethical and veterinary committee of the Canton of Vaud, Switzerland. As was described previously[29], mice were deeply anesthetised by intra-peritoneal injection of 50mg/kg sodium pentobarbital prior to a transcardiac perfusion of 10ml heparinised PBS (5 I.U./ml Liquemin). Tissues were fixed by perfusing with 10ml of freshly-prepared 4% paraformaldehyde (CAS 30525-89-4, Carl Roth AG 0964.1) and an overnight post-fixation step at 4°C.

5.2 Sample preparation

All the following steps took place in the dark. Samples were washed for 30 minutes in PBS after the overnight fixation. A 45-minute step-wise dehydration in methanol precedes overnight autofluorescence quenching in a 2:1:3 ratio solution of MetOH:DMSO:H_2O_2 overnight at room temperature. The samples are washed twice in pure MetOH in preparation for three freeze-thaw cycles between -80°C and room temperature (1 hour and 30 minute cycles respectively) in order to permeabilize the tissue before antibody-mediated staining. A step-wise rehydration to TBS-Tween prepares the samples for antibody-mediated staining of targets. This begins with blocking for 24h, is followed by a primary antibody incubation for 48h and a 24h washing step and ends with a 48h incubation in a secondary antibody and a final 24h washing step. To stain immune cells, we used a rat anti-mouse CD45 monoclonal antibody conjugated to APC (BioLegend 147708) and a goat anti-rat IgG (H+L) Alexa Fluor 647 (Invitrogen A21247).

The samples were mounted in custom cylindrical moulds in 1.5% agarose, dehydrated in pure methanol (CAS 67-56-1, Sigma-Aldrich 322415) for 24 hours and rehydrated in a 1:2 benzyl alcohol:benzyl benzoate mixture for a minimum of 48h before acquisition (BA: CAS 100-51-6, Sigma-Aldrich 305197; BB: CAS 120-51-4, Sigma-Aldrich B6630).

5.3 Microscopy

OPT

Detailed descriptions of the optical setup are available at Schmidt, C. *et al.* (2021)[29]. Multi-channel sets of projections were acquired first with a 625nm LED (filtered within a 595 nm and 645 nm range, AT620/50x, Chroma) for the CD45 positive signal followed by a 415nm LED (400-440nm filter range, AT420/40x, Chroma) to acquire tissue autofluorescence. In each channel, either 400 or 1200 projections

were acquired and subsequently reconstructed using our version of the filtered back-projection algorithm[29]. Reconstructed stacks were cropped in ImageJ[66] and visualised in 3D.

Reverse-OPT

After OPT imaging, the samples were dehydrated in pure methanol and rehydrated in PBS for 24h each. At this stage, it is possible to carefully track regions of interest identified in the 3D OPT images to be specifically observed using other imaging modalities downstream. The samples were extracted from the agarose moulds and frozen in optimal cutting temperature (OCT) medium on dry ice. Using a Leica CM3050S cryostat, 25 micrometre-thick sections were collected and mounted on coated glass slides (Epredia™ J1800AMNZ). The sections were counterstained with DAPI (Thermofisher D1306) at a concentration of 5µg/ml for 10 minutes with a 5 minute pre- and post-wash with 0.3% Triton-X100 in PBS.

Confocal microscopy

Confocal microscopy was performed using a Leica SP8 inverted microscope, producing two-channel images encompassing the CD45-positive and nuclei signals. Sequential acquisition began with the AlexaFluor647 channel followed by the DAPI channel. Exposure times were determined according to live observation of pixel intensities in order to avoid over-exposure of the tissue. Tiled acquisitions of whole-gut sections were performed using the automated tile function in the LAS-X software.

5.4 Image Processing

Virtual unfolding

The image processing pipeline for virtual unfolding was inspired by previous reports[30] applied using Fiji and is available in the form of a macro algorithm. All steps outlined below are applied to all of the sections within the filtered-back-projection stacks. First, the gut tissue is segmented from the lumen and surrounding background and a mask is created. For each section, the segmented tissue outline is added to the ROI manager. The centroid coordinates within the tissue outline are calculated and used as an origin for the identification of a sectioning origin at a 45° angle from the centre. From this point, we interpolate a polygon shape to draw the line along which the unfolding takes place. A stack of the straightened images is produced and re-sliced orthogonally to create the unfolded image whose field of view include the entire surface of the sample, spanning the lumen in the innermost slice to the outermost layers of the gut. From this image, the apex of each villus is identified by applying a Laplacian filter and extracting local maxima ROIs, whose density can then be calculated within a defined area.

ILF segmentation

Quantifiable characteristics were extracted from FBP reconstructions showing the isolated lymphoid follicles using the surface tool in Imaris. The smoothing of surface areas was set to 2µm and thresholding based on absolute intensity, whose values were set visually by the user. Larger structures

were segmented by implementing the “number of voxels” filter. Volume and distance statistics were exported in csv format for data plotting.

Declarations

Funding. H2020 Framework Program of the European Union (grant no 686271) and Innosuisse (grant no 31434.1 IP-ICT).

Acknowledgments. The authors are grateful to Theo Lasser for useful discussions and overall support and to BIOP imaging facility for technical support and access to confocal microscopes. The Clean Mouse Facility is supported by the Genaxen Foundation, Inselspital and the University of Bern.

Disclosures. The authors declare no conflicts of interest.

Data availability. Data and code underlying the results presented in this paper are available on website srm.epfl.ch.

References

1. Belkaid, Y. & Harrison, O. J. Homeostatic Immunity and the Microbiota. *Immunity* **46**, 562–576 (2017).
2. Zheng, D., Liwinski, T. & Elinav, E. Interaction between microbiota and immunity in health and disease. *Cell Res.* **30**, 492–506 (2020).
3. Zhao, Q. & Elson, C. O. Adaptive immune education by gut microbiota antigens. *Immunology* **154**, 28–37 (2018).
4. De Agüero, M. G. *et al.* The maternal microbiota drives early postnatal innate immune development. *Science (80-.).* **351**, 1296–1302 (2016).
5. Muscogiuri, G. *et al.* Gut microbiota: a new path to treat obesity. *Int. J. Obes. Suppl.* **9**, 10–19 (2019).
6. Gurung, M. *et al.* EBioMedicine Role of gut microbiota in type 2 diabetes pathophysiology. *EBioMedicine* **51**, 102590 (2020).
7. Zhang, X., Chen, B. di, Zhao, L. dan & Li, H. The Gut Microbiota: Emerging Evidence in Autoimmune Diseases. *Trends Mol. Med.* **26**, 862–873 (2020).
8. Wypych, T. P., Wickramasinghe, L. C. & Marsland, B. J. The influence of the microbiome on respiratory health. *Nat. Immunol.* **20**, 1279–1290 (2019).
9. Ubags, N. D. *et al.* Microbiome-induced antigen-presenting cell recruitment coordinates skin and lung allergic inflammation. *J. Allergy Clin. Immunol.* **147**, 1049-1062.e7 (2021).
10. Skjerven, H. O. *et al.* Skin emollient and early complementary feeding to prevent infant atopic dermatitis (PreventADALL): a factorial, multicentre, cluster-randomised trial. *Lancet* **395**, 951–961

(2020).

11. Zhang, L. *et al.* Near infrared readouts offer sensitive and rapid assessments of intestinal permeability and disease severity in inflammatory bowel disease models. *Sci. Rep.* **10**, 1–12 (2020).
12. Moussata, D. *et al.* Confocal laser endomicroscopy is a new imaging modality for recognition of intramucosal bacteria in inflammatory bowel disease in vivo. *Gut* **60**, 26–33 (2011).
13. Rath, T., Dieterich, W., Kätscher-Murad, C., Neurath, M. F. & Zopf, Y. Cross-sectional imaging of intestinal barrier dysfunction by confocal laser endomicroscopy can identify patients with food allergy in vivo with high sensitivity. *Sci. Rep.* **11**, 1–9 (2021).
14. Xie, Y. *et al.* Impact of a high-fat diet on intestinal stem cells and epithelial barrier function in middle-aged female mice. *Mol. Med. Rep.* **21**, 1133–1144 (2020).
15. Park, C. *et al.* Obesity Modulates Intestinal Intraepithelial T Cell Persistence, CD103 and CCR9 Expression, and Outcome in Dextran Sulfate Sodium–Induced Colitis. *J. Immunol.* **203**, 3427–3435 (2019).
16. Joesten, W. C., Short, A. H. & Kennedy, M. A. Spatial variations in gut permeability are linked to type 1 diabetes development in non-obese diabetic mice. *BMJ Open Diabetes Res. Care* **7**, 1–9 (2019).
17. Eberl, G. & Lochner, M. The development of intestinal lymphoid tissues at the interface of self and microbiota. *Mucosal Immunol.* **2**, 478–485 (2009).
18. Mowat, A. M. & Agace, W. W. Regional specialization within the intestinal immune system. *Nat. Rev. Immunol.* **14**, 667–685 (2014).
19. Bouskra, D. *et al.* Lymphoid tissue genesis induced by commensals through NOD1 regulates intestinal homeostasis. *Nature* **456**, 507–510 (2008).
20. Fenton, T. M. *et al.* Immune Profiling of Human Gut-Associated Lymphoid Tissue Identifies a Role for Isolated Lymphoid Follicles in Priming of Region-Specific Immunity. *Immunity* **52**, 557-570.e6 (2020).
21. Jørgensen, P. B. *et al.* Identification, isolation and analysis of human gut-associated lymphoid tissues. *Nat. Protoc.* **16**, 2051–2067 (2021).
22. Welch, J. L. M., Hasegawa, Y., McNulty, N. P., Gordon, J. I. & Borisy, G. G. Spatial organization of a model 15-member human gut microbiota established in gnotobiotic mice. *Proc. Natl. Acad. Sci. U. S. A.* **114**, E9105–E9114 (2017).
23. Parthasarathy, R. Monitoring microbial communities using light sheet fluorescence microscopy. *Curr. Opin. Microbiol.* **43**, 31–37 (2018).
24. Lee, K. J. I. *et al.* Macro optical projection tomography for large scale 3D imaging of plant structures and gene activity. *J. Exp. Bot.* **68**, 527–538 (2017).
25. Eriksson, A. U. *et al.* Near infrared optical projection tomography for assessments of β-cell mass distribution in diabetes research. *J. Vis. Exp.* 1–11 (2013). doi:10.3791/50238
26. Lindsey, B. W. & Kaslin, J. Optical projection tomography as a novel method to visualize and quantitate whole-brain patterns of cell proliferation in the adult zebrafish brain. *Zebrafish* **14**, 574–577 (2017).

27. Nieman, B. J., Wong, M. D. & Henkelman, R. M. Genes into geometry: Imaging for mouse development in 3D. *Curr. Opin. Genet. Dev.* **21**, 638–646 (2011).
28. Nguyen, D. *et al.* Optical projection tomography for rapid whole mouse brain imaging. *Biomed. Opt. Express* **8**, 5637 (2017).
29. Schmidt, C. *et al.* High resolution optical projection tomography platform for multispectral imaging of the mouse gut. *Biomed. Opt. Express* **12**, 3619–3629 (2021).
30. Maiuri, L. *et al.* Virtual unfolding of light sheet fluorescence microscopy dataset for quantitative analysis of the mouse intestine. *J. Biomed. Opt.* **21**, 1 (2016).
31. Round, J. L. & Mazmanian, S. K. The gut microbiota shapes intestinal immune responses during health and disease. *Nat. Rev. Immunol.* **9**, 313–323 (2009).
32. Burcelin, R. Gut microbiota and immune crosstalk in metabolic disease. *Mol. Metab.* **5**, 771–781 (2016).
33. Sittipo, P., Lobionda, S., Lee, Y. K. & Maynard, C. L. Intestinal microbiota and the immune system in metabolic diseases. *J. Microbiol.* **56**, 154–162 (2018).
34. Wu, H. J. & Wu, E. The role of gut microbiota in immune homeostasis and autoimmunity. *Gut Microbes* **3**, 4–14 (2012).
35. Garcia-Gutierrez, E., Narbad, A. & Rodríguez, J. M. Autism Spectrum Disorder Associated With Gut Microbiota at Immune, Metabolomic, and Neuroactive Level. *Front. Neurosci.* **14**, 1–14 (2020).
36. Main, B. S. & Minter, M. R. Microbial immuno-communication in neurodegenerative diseases. *Front. Neurosci.* **11**, 1–8 (2017).
37. Takiishi, T., Fenero, C. I. M. & Câmara, N. O. S. Intestinal barrier and gut microbiota: Shaping our immune responses throughout life. *Tissue Barriers* **5**, (2017).
38. Rhee, K.-J., Sethupathi, P., Driks, A., Lanning, D. K. & Knight, K. L. Role of Commensal Bacteria in Development of Gut-Associated Lymphoid Tissues and Preimmune Antibody Repertoire. *J. Immunol.* **172**, 1118–1124 (2004).
39. Knoop, K. A. & Newberry, R. D. Isolated lymphoid follicles are dynamic reservoirs for the induction of intestinal IgA. *Front. Immunol.* **3**, 1–7 (2012).
40. Mörbe, U. M. *et al.* Human gut-associated lymphoid tissues (GALT); diversity, structure, and function. *Mucosal Immunol.* **14**, 793–802 (2021).
41. Fu, Y. Y., Peng, S. J., Lin, H. Y., Pasricha, P. J. & Tang, S. C. 3-D imaging and illustration of mouse intestinal neurovascular complex. *Am. J. Physiol. - Gastrointest. Liver Physiol.* **304**, 1–11 (2013).
42. Li, T. *et al.* Multiscale imaging of colitis in mice using confocal laser endomicroscopy, light-sheet fluorescence microscopy, and magnetic resonance imaging. *J. Biomed. Opt.* **24**, 1 (2019).
43. Zundler, S. *et al.* Three-Dimensional Cross-Sectional Light-Sheet Microscopy Imaging of the Inflamed Mouse Gut. *Gastroenterology* **153**, 898–900 (2017).
44. Dumur, T. *et al.* Probing the 3D architecture of the plant nucleus with microscopy approaches: challenges and solutions. *Nucleus* **10**, 181–212 (2019).

45. Ballabeni, A., Apollonio, F. I., Gaiani, M. & Remondino, F. Advances in image pre-processing to improve automated 3d reconstruction. *Int. Arch. Photogramm. Remote Sens. Spat. Inf. Sci. - ISPRS Arch.* **40**, 315–323 (2015).
46. Kalinin, A. A. *et al.* 3D Shape Modeling for Cell Nuclear Morphological Analysis and Classification. *Sci. Rep.* **8**, 1–14 (2018).
47. Bhattacharjee, S., Satwaha, S., Thornton, K. & Scholz, D. Label-Free Imaging and Optical Characterization of Tissues Based on Autofluorescence. *ACS Omega* **3**, 5926–5930 (2018).
48. Fritscher-Ravens, A. *et al.* Confocal endomicroscopy shows food-associated changes in the intestinal mucosa of patients with irritable bowel syndrome. *Gastroenterology* **147**, 1012-1020.e4 (2014).
49. Abadie, V. *et al.* IL-15, gluten and HLA-DQ8 drive tissue destruction in coeliac disease. *Nature* **578**, 600–604 (2020).
50. Gibiino, G., Lopetuso, L., Ricci, R., Gasbarrini, A. & Cammarota, G. Coeliac disease under a microscope: Histological diagnostic features and confounding factors. *Comput. Biol. Med.* **104**, 335–338 (2019).
51. Rooks, M. G. & Garrett, W. S. Gut microbiota, metabolites and host immunity. *Nat. Rev. Immunol.* **16**, 341–352 (2016).
52. Levy, M., Kolodziejczyk, A. A., Thaiss, C. A. & Elinav, E. Dysbiosis and the immune system. *Nat. Rev. Immunol.* **17**, 219–232 (2017).
53. Maloy, K. J. & Powrie, F. Intestinal homeostasis and its breakdown in inflammatory bowel disease. *Nature* **474**, 298–306 (2011).
54. D'Addio, F. & Fiorina, P. Type 1 Diabetes and Dysfunctional Intestinal Homeostasis. *Trends Endocrinol. Metab.* **27**, 493–503 (2016).
55. Kim, S. *et al.* Transneuronal Propagation of Pathologic α-Synuclein from the Gut to the Brain Models Parkinson's Disease. *Neuron* **103**, 627-641.e7 (2019).
56. Blacher, E. *et al.* Potential roles of gut microbiome and metabolites in modulating ALS in mice. *Nature* **572**, 474–480 (2019).
57. Sgritta, M. *et al.* Mechanisms Underlying Microbial-Mediated Changes in Social Behavior in Mouse Models of Autism Spectrum Disorder. *Neuron* **101**, 246-259.e6 (2019).
58. Benakis, C. *et al.* Commensal microbiota affects ischemic stroke outcome by regulating intestinal γδ T cells. *Nat. Med.* **22**, 516–523 (2016).
59. Hermiston, M. L., Xu, Z. & Weiss, A. CD45: A critical regulator of signaling thresholds in immune cells. *Annu. Rev. Immunol.* **21**, 107–137 (2003).
60. Sawai, C. M. *et al.* Hematopoietic Stem Cells Are the Major Source of Multilineage Hematopoiesis in Adult Animals. *Immunity* **45**, 597–609 (2016).
61. Hooper, L. V. & MacPherson, A. J. Immune adaptations that maintain homeostasis with the intestinal microbiota. *Nat. Rev. Immunol.* **10**, 159–169 (2010).

62. Donaldson, D. S., Bradford, B. M., Artis, D. & Mabbott, N. A. Reciprocal regulation of lymphoid tissue development in the large intestine by IL-25 and IL-23. *Mucosal Immunol.* **8**, 582–595 (2015).
63. Bosco, N. & Noti, M. The aging gut microbiome and its impact on host immunity. *Genes Immun.* (2021). doi:10.1038/s41435-021-00126-8
64. Belkaid, Y. & Hand, T. W. Role of the microbiota in immunity and inflammation. *Cell* **157**, 121–141 (2014).
65. Round, J. L. & Mazmanian, S. K. The gut microbiota shapes intestinal immune responses during health and disease. *Nat. Rev. Immunol.* **9**, 600–600 (2009).
66. Schindelin, J., Rueden, C. T., Hiner, M. C. & Eliceiri, K. W. The ImageJ ecosystem: An open platform for biomedical image analysis. *Mol. Reprod. Dev.* **82**, 518–529 (2015).

Figures

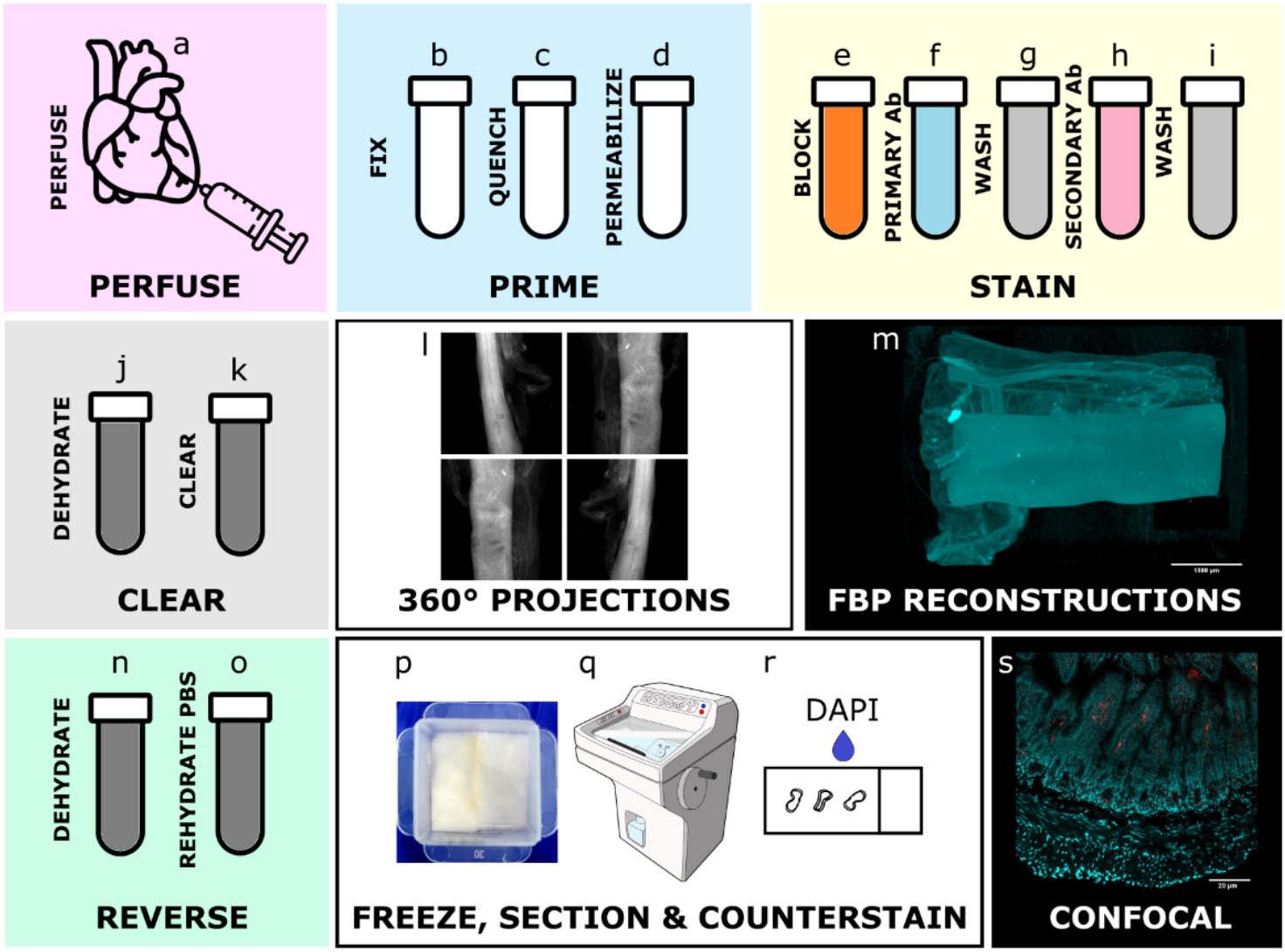

Figure 1

gutOPT workflow. Sample preparation and handling in four steps: sample preparation (a-k), imaging and image processing (l-m), reverse OPT (n-r) and secondary imaging (s). The experimental steps for sample preparation are: transcardiac perfusion of PBS and 4% PFA (a); 4-hour PFA fixation (b); overnight autofluorescence quenching with methanol, DMSO and hydrogen peroxide 1:3:2 mixture (c); permeabilisation by three freeze-thaw cycles between -80°C (1h) and room temperature (30min) (d); 24-hour tissue blocking (e); 48-hour primary antibody incubation (f); 24-hour wash (g); 48-hour secondary antibody incubation (h); 24-hour wash (j); 36-hour dehydration in pure methanol with two solution changes (j) and clearing in 1:2 ratio of benzyl alcohol and benzyl benzoate (k). Optical projections are acquired over a 360° rotation of the sample (i) and a 3D image is reconstructed using filtered back projection (m). OPT processing may be reversed in order to image sections of the same sample using alternative imaging modalities. To do so, samples are dehydrated in pure methanol for 36 hours (n), rehydrate in PBS (o), mounted in cryomatrix (p), cryo-sectioned (q) and counterstained with DAPI (r). High-resolution imaging modalities such as confocal microscopy (s) may be applied to samples whose large-scale volume has been observed.

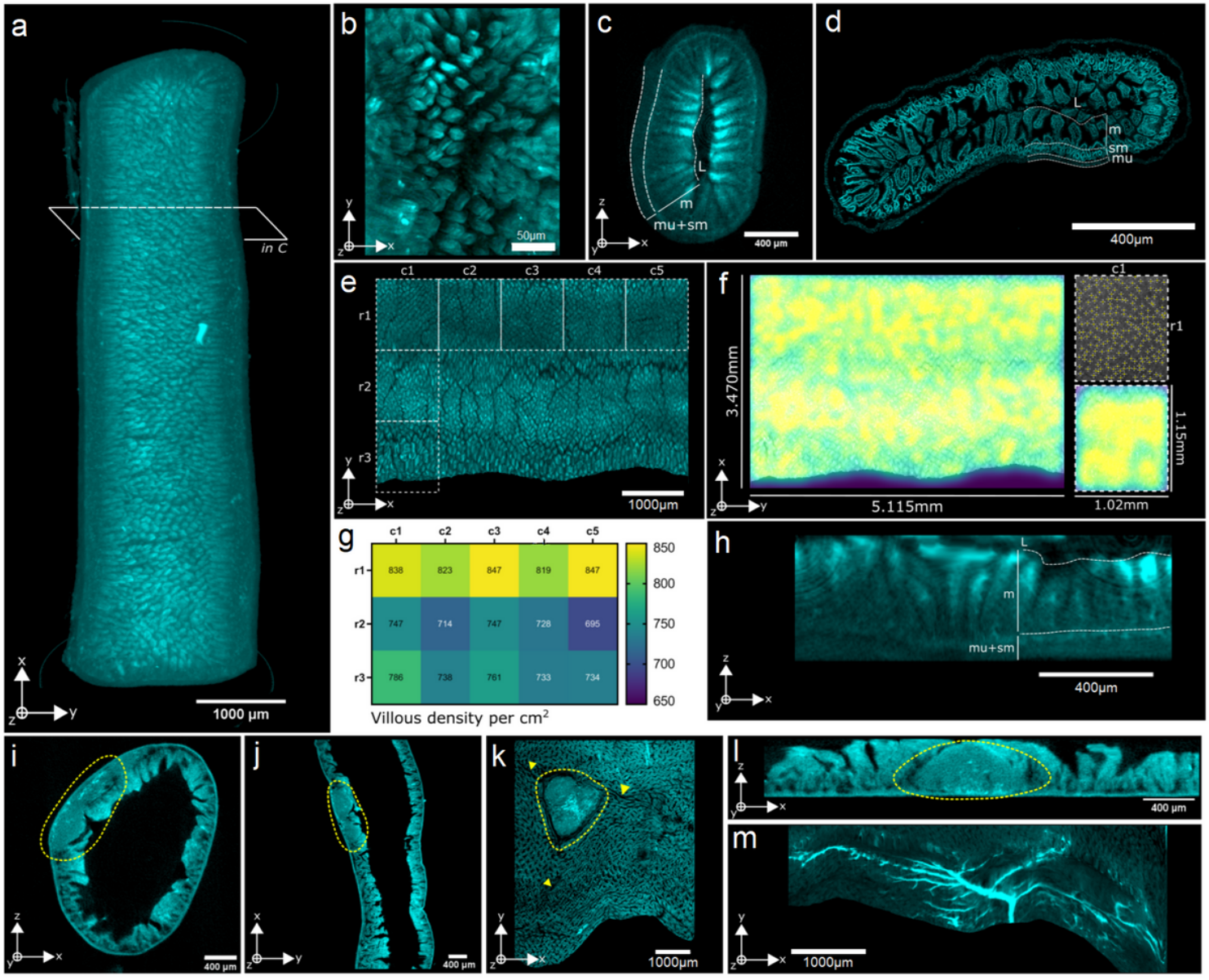

Figure 2

Visualization and characterization of the autofluorescence signal. (a) FBP reconstruction from a single acquisition of gut in the autofluorescence channel. (b) Close-up of the villi structures from within the lumen. (c) Cross-sectional view of the 3D reconstruction, with visible layers labelled mu = muscularis, sm = submucosa, m = mucosa and L = lumen. (d) High-resolution tiled acquisition of the same gut sample using confocal microscopy, with concurrent layers labelled. (e) Innermost layer of the same reconstruction that was virtually unfolded30. (f) Use of unfolded image to perform whole gut segment quantification of villus density by applying a Laplacian filter and the find maxima function. (g) Villi density quantified within sub-regions of the unfolded scan. (h) Cross-sectional view of unfolded image, with mucosal layers labelled as before. (i-m) Images of secondary lymphoid structures from a cross-section view (i and j) or top to bottom (l) (encircled in yellow). (j) Side view of the same structure as in I. (k) Unfolded image reveals tri-lobular structure and possible vascularisation (arrow). (l) Straightened cross section of structure in i. (m) Widespread network of large vessels in an unfolded image.

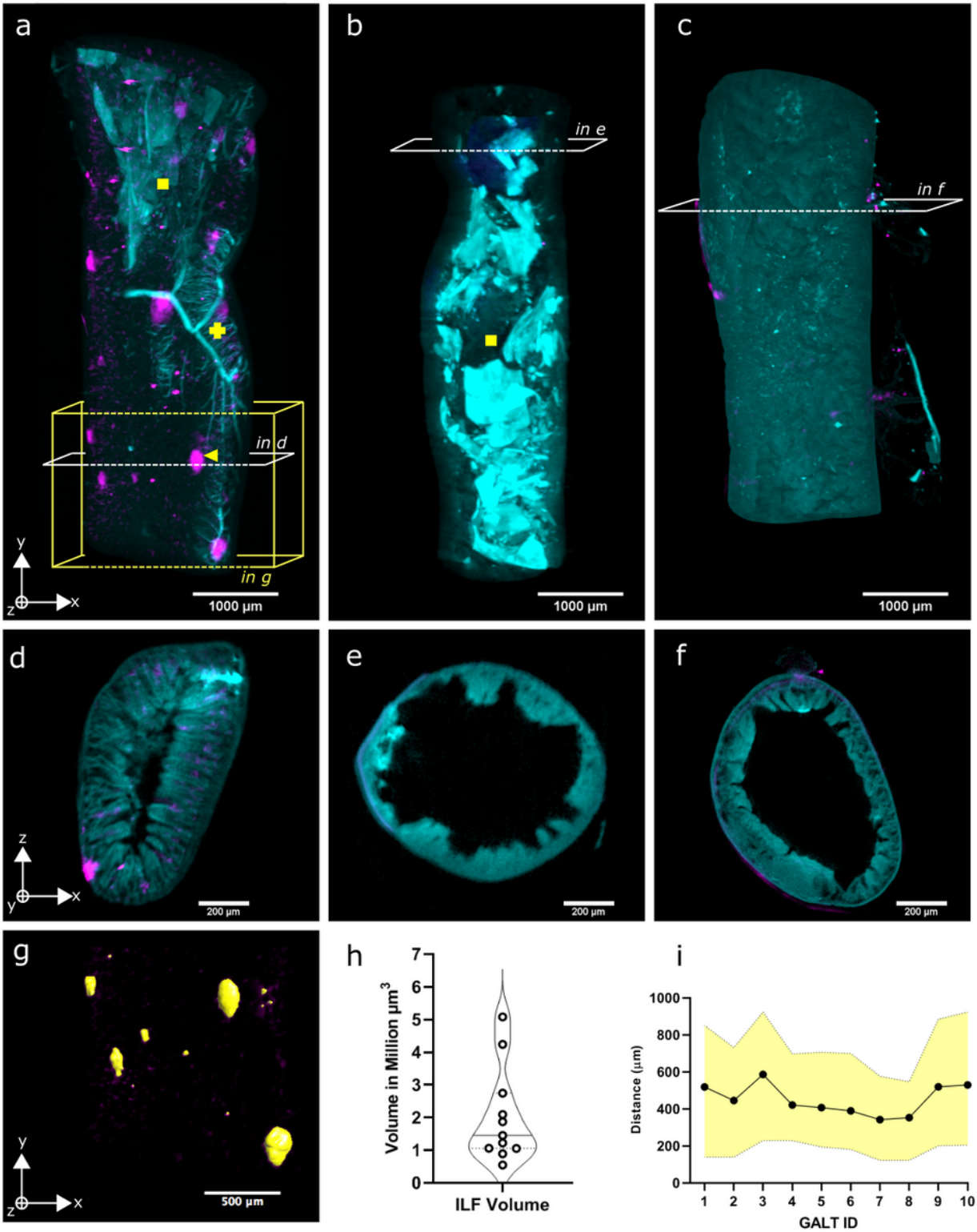

Figure 3

Multi-channel OPT reconstructions and segmentation of gut immune component. (a-c) Longitudinal views of two-channel OPT renders with tissue autofluorescence in cyan and CD45-positive cell clusters in magenta. Age- and microbiota-dependent development of gut-associated lymphoid structures (GALTs) is evident in a healthy adult SPF gut (a) versus young SPF (b) and adult germ-free (c) gut samples. Structures of interest include the positive cell clusters (triangle), vascular network (cross) and luminal

dietary fibers (square). (d-f) Cross-sectional view of 3D reconstructions for samples shown A-D. (g) 3D segmentation of isolated lymphoid follicles (ILFs) signal observed in box shown in (a). (h) The measured volume occupied by individual CD45-positive regions in a healthy old C57BL6 mouse, measured in million-µm3. (i) Spatial distribution of ILFs throughout the tissue seen in A as measured by minimum, mean and maximum distance in µm between each follicle.

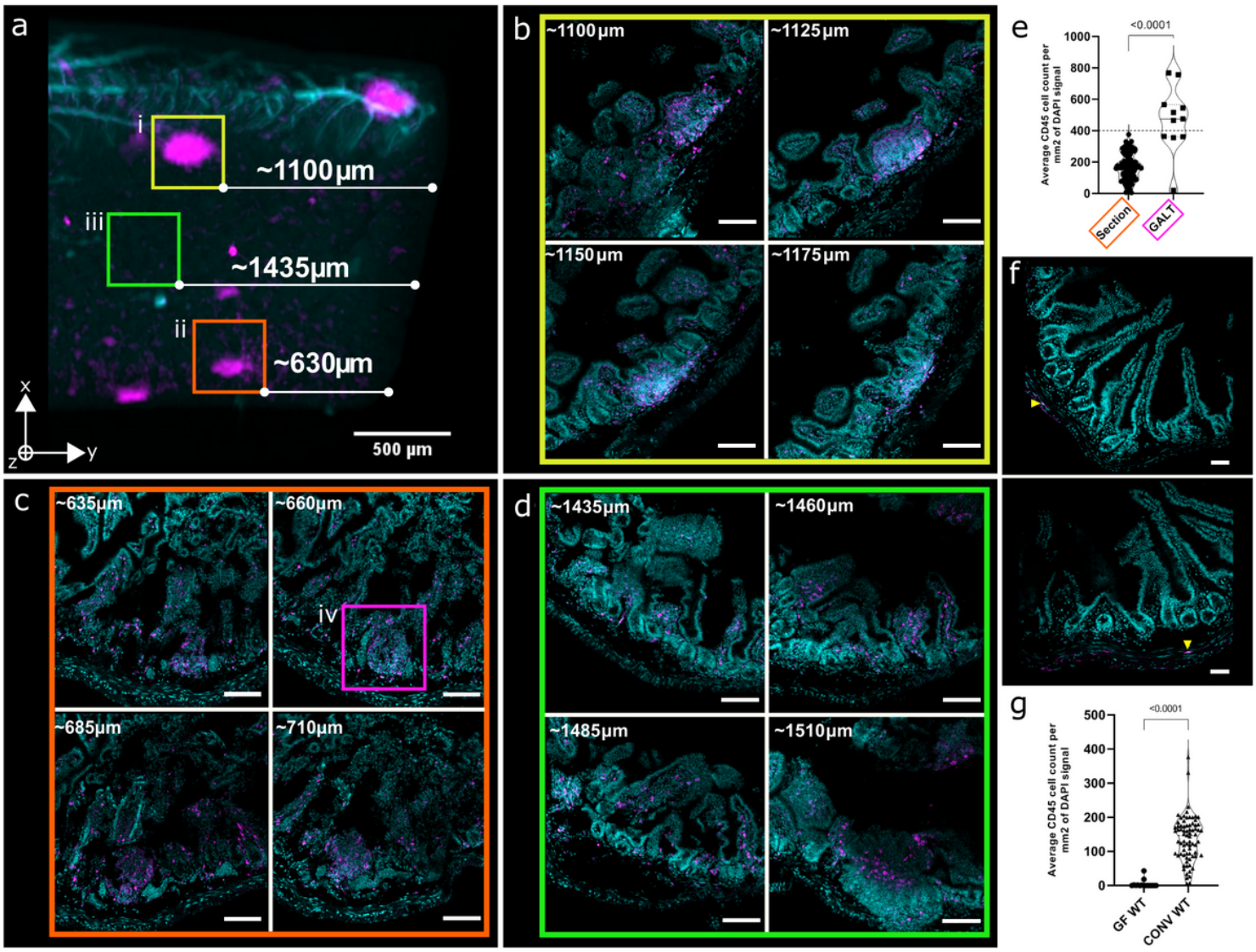

Figure 4

Reverse OPT for tracking of ROIs in high-resolution imaging modalities. (a) Close-up and selection of two GALT ROIs in OPT reconstruction, with calculation of distance from the end of the tissue. Regions i-iii are regions shown in b-d, with sectors i and ii containing CD45 signal and iii being empty. (b-d) Scale bars are 200µm. (b) Two-channel confocal images of reverse-OPT sections within the depth of (i) in (a), with distance from the end of the tissue calculated based on the number of 25 µm-thick sections collected. Nuclei were stained with DAPI and CD45 signal comes from pre-OPT staining. High CD45+ cell density regions are the ILFs visible by OPT and are surrounded by sparse CD45+ cells. (c) Confocal depths in the second ROI (ii) selected in (a). (d) Confocal depth in a region with no observed ILFs in (a) showing only sparse CD45 signal. (a-d) Images come from a healthy SPF adult mouse gut. (e) Comparison of CD45-

positive cell density within GALT region and surrounding tissue measured in sections from four gut samples. The signal density threshold above which structures are visible in OPT reconstructions is estimated at 400 fluorescent cells/mm2 of DAPI signal. (f) Confocal acquisitions from an old germ-free mouse gut, with no ILF signal observed in OPT and a visibly reduced presence of CD45-positive cells throughout the tissue. Scale bars are 200μm. (g) Comparison of whole-section area density of CD45-positive cells in SPF and germ-free gut samples (example images b-d and f), showing significant reduction in immune cell presence in the gut lining of germ-free animals.

Supplementary Files

This is a list of supplementary files associated with this preprint. Click to download.

- SupplementaryInformation.pdf
- OPT2movie.mp4